

Generalization of Benalcazar-Bernevig-Hughes model to arbitrary dimensions

Xun-Jiang Luo¹ and Fengcheng Wu^{1,2,*}

¹*School of Physics and Technology, Wuhan University, Wuhan 430072, China*

²*Wuhan Institute of Quantum Technology, Wuhan 430206, China*

The Benalcazar-Bernevig-Hughes (BBH) model [Science **357**, 61 (2017)], featuring bulk quadrupole moment, edge dipole moments, and corner states, is a paradigm of both higher-order topological insulators and topological multipole insulators. In this work, we generalize the BBH model to arbitrary dimensions by utilizing the Clifford algebra. For the generalized BBH model, the analytical solution of corner states can be directly constructed in a unified way. Based on the solution of corner states and chiral symmetry analysis, we develop a general boundary projection method to extract the boundary Hamiltonians, which turns out to be the BBH models of lower dimension and reveals the dimensional hierarchy.

I. INTRODUCTION

The past few years have witnessed the rapid development of higher-order topological phases (HOTPs) [1–39], which include insulators [40–46], superconductors [47–60], and semi-metals [61–63]. In a d -dimensional (dD) system, an n th-order topological phase features robust gapless states at its $(d - n)D$ boundaries. For example, the second- and third-order topological phases in 3D host robust hinge states and corner states, respectively. The corner states in a system with chiral or particle-hole symmetry stay at exact zero energy, which can give rise to fractional corner charges in insulators [64–66] and non-Abelian anyons in superconductors [67–70]. These exotic topological properties of HOTPs attract much attention.

A typical example of HOTPs is the Benalcazar-Bernevig-Hughes (BBH) model [1, 2], which features corner states and bulk quadrupole moment (a quantity that generalizes the electric dipole moment to 2D) [1, 2]. The 3D and 4D counterparts of the 2D BBH model, which host bulk octupole and hexadecapole moments, respectively, have also been studied [1, 2, 71]. Particularly, the 2D, 3D, and 4D BBH models have been experimentally realized in artificial systems, including phononic crystals [72–74], acoustic crystals [75, 76], and electrical circuits [77–80]. An interesting question is how to generalize the BBH model to arbitrary dimensions.

The BBH model, as a kind of higher-dimensional generalization of the 1D Su-Schrieffer-Heeger (SSH) model [81], exhibits dimensional hierarchy. The bulk quadrupole (octupole) moment of the 2D (3D) BBH model manifest themselves by the presence of edge dipole (surface quadrupole and hinge dipole moments), as schematically shown in Fig. 1(a) (Fig. 1(b)). In the seminal papers of Refs. 1 and 2, the nested Wilson loop method was developed to reveal boundary-localized multipole moment by exploring the Wannier band topology. However, this method increases its computational complexity sharply with the increasing of the dimension of the system. An alternative way of revealing the boundary

localized multipole moments of the BBH model is to directly extract the boundary Hamiltonians of the system. For instance, the edge dipole moments in the 2D BBH model can be unveiled by its edge Hamiltonians, which turn out to be a two-band SSH model hosting dipole moment [82, 83]. Similarly, the surface quadrupole moments and hinge dipole moments of the 3D BBH model can be revealed by the surface and hinge Hamiltonians of the system, respectively. Therefore, the key point of uncovering the dimensional hierarchy of the BBH model is to analytically derive the boundary Hamiltonians through boundary projection in a systematic and generalized way.

In this work, we generalize the BBH model to arbitrary dimensions and present a unified Hamiltonian form, which is the summation of the extended Su-Schrieffer-Heeger (SSH) model (multi copies of the two-band SSH model) along different directions. Based on the thorough investigation of the 1D extended SSH model enabled by chiral symmetry analysis, we directly construct the analytical solution of corner states in a unified way. Based on the solution of corner states, we further develop a general boundary projection method to derive the boundary Hamiltonians for an arbitrary dimensional system, which turns out to be the BBH model of lower dimension and reveals the dimensional hierarchy.

The rest of this paper is organized as follows. In Sec. II, we introduce the 1D extended SSH model. In Sec. III, we generalize the BBH model to arbitrary dimensions and construct the analytical solution of corner states. In Sec. IV, we perform boundary projection analysis and extract the boundary Hamiltonians. In Sec. V, we conclude with a discussion and summary. Appendices A–C complement the main text with additional technical details.

II. 1D EXTENDED SSH MODEL

We start our discussion by introducing the 1D extended SSH model, which will be used as a building block to construct the Hamiltonians of the BBH model in arbitrary dimensions. The Bloch Hamiltonian of the 1D

* wufcheng@whu.edu.cn

extended SSH model is

$$h(k) = (t + \lambda \cos k)\gamma_a^{(d)} + \lambda \sin k\gamma_b^{(d)}, \quad (1)$$

where t and λ are model parameters and k denotes the momentum. In Eq. (1), $\gamma_a^{(d)}$ and $\gamma_b^{(d)}$ are $2^d \times 2^d$ anti-commuting Gamma matrices (see Appendix A),

$$\{\gamma_a^{(d)}, \gamma_b^{(d)}\} = 0, \quad (\gamma_a^{(d)})^2 = (\gamma_b^{(d)})^2 = 1. \quad (2)$$

The chiral symmetry of h is explicitly defined by $C = i\gamma_a^{(d)}\gamma_b^{(d)}$ which satisfies $\{C, h\} = 0$. Therefore, 1D Hamiltonian h belongs to the AIII symmetry class and has a Z topological classification [84–86].

To clearly display the topology of h , which does not depend on the representation of matrices $\gamma_a^{(d)}$ and $\gamma_b^{(d)}$, without loss of generality, we choose

$$\gamma_a^{(d)} = \sigma_2 \otimes \underbrace{\sigma_0 \cdots \sigma_0}_{d-1}, \quad \gamma_b^{(d)} = \sigma_1 \otimes \underbrace{\sigma_0 \cdots \sigma_0}_{d-1}, \quad (3)$$

where $\sigma_{1,2}$ are Pauli matrices and σ_0 is a 2×2 identify matrix. Following Eq. (3), h is composed of 2^{d-1} blocks and each block behaves as a two-band SSH model. When $|t| < |\lambda|$, h is topologically nontrivial and characterized by the winding number $\nu = 2^{d-1}$, as explicitly shown in Appendix B.

In the open boundary condition, h hosts 2^{d-1} end zero-energy states (EZESs) at each end owing to the bulk-boundary correspondence. The EZESs solution of h can be analytically derived by directly solving the differential equation $h(r)|X_\alpha(r)\rangle = 0$ (see Appendix B). Here, the low-energy Hamiltonian $h(r)$ is obtained by expanding $h(k)$ at $k = 0$ to the second order of k and replacing $k = -i\partial_r$, where r is the 1D position coordinate. The EZESs are the eigenstates of chiral symmetry

$$C = i\gamma_a^{(d)}\gamma_b^{(d)} = \sigma_z \otimes \underbrace{\sigma_0 \cdots \sigma_0}_{d-1}, \quad (4)$$

which has the eigenvalue $z = \pm 1$. The EZESs labeled by $z = -1$ and $z = 1$ are localized close to end $r = 0$ and $r = L$, respectively, where L is the length of the 1D system. Therefore, the wave function of the 1D EZESs takes the form

$$|X_z(r)\rangle = f_z(r)|\psi_z\rangle, \quad (5)$$

where 2^d -component spinor $|\psi_z\rangle$ satisfies $C|\psi_z\rangle = z|\psi_z\rangle$ and $f_+(r)$ and $f_-(r)$ are the real space localized wave function determined by parameters t and λ .

We note that the topology of h does not depend on the given representations of $\gamma_a^{(d)}$ and $\gamma_b^{(d)}$. In Appendix B, we calculate the winding number and EZESs wave function of h for a general case.

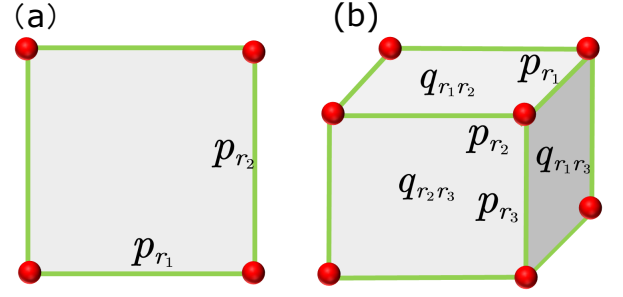


FIG. 1. (a) Schematic illustration for the edge dipole moments (p_{r_1}, p_{r_2}) of topological quadrupole insulators. (b) Schematic illustration for the surface quadrupole moments ($q_{r_1 r_2}, q_{r_1 r_3}, q_{r_2 r_3}$) and hinge dipole moments ($p_{r_1}, p_{r_2}, p_{r_3}$) of topological octupole insulators.

III. HAMILTONIANS AND CORNER STATES

A. Model Hamiltonians

Lower-dimensional topological states can be used to construct topological phases in higher dimensions [87–89]. Here, we choose the 1D extended SSH model as the building block and construct the dD Hamiltonians

$$\mathcal{H}_d(\mathbf{k}_d) = \sum_{s=1}^d h_s(k_s), \quad (6)$$

$$h_s(k_s) = M_s(k_s)\gamma_{sa}^{(d)} + \lambda_s \sin k_s \gamma_{sb}^{(d)},$$

where $\mathbf{k}_d = (k_1, \dots, k_d)$ is the dD momentum vector, s labels the different directions, $M_s(k_s) = (t_s + \lambda_s \cos k_s)$ with t_s and λ_s being model parameters, and h_s is the 1D extended SSH model introduced in Sec. II, respecting the chiral symmetry $C_s = i\gamma_{sa}^{(d)}\gamma_{sb}^{(d)}$. The $2^d \times 2^d$ matrices $\{\gamma_{1a, \dots, da, 1b, \dots, db}^{(d)}\}$ form the Clifford algebra $\{\gamma_j^{(d)}, \gamma_{j'}^{(d)}\} = 2\delta_{jj'}$ for $j, j' \in \{1a, \dots, da, 1b, \dots, db\}$. The energy spectrum of \mathcal{H}_d is

$$E = \pm \sqrt{\sum_{s=1}^d E_s^2}, \quad E_s = \sqrt{M_s^2(k_s) + (\lambda_s \sin k_s)^2}, \quad (7)$$

where $\pm E_s$ is the energy spectrum of h_s . Therefore, the bulk energy spectrum of \mathcal{H}_d is fully gapped unless $|t_s| = |\lambda_s|$ for $s = 1, \dots, d$. Hereafter, we take $|t_s| < |\lambda_s|$ unless otherwise stated.

For the cases $d = 1, 2, 3, 4$, Hamiltonians \mathcal{H}_d obtained by considering the concrete Gamma matrices representation have been previously studied [1, 2, 71, 80]. The bulk quadrupole ($d = 2$), octupole ($d = 3$), and hexadecapole ($d = 4$) moments were identified by calculating the nested Wilson loop invariants. In Eq. (6), we generalize the BBH model to arbitrary dimensions from the perspective of Gamma matrices.

B. Corner zero-energy states

The BBH model hosts corner zero-energy states (CZESs), which are usually verified by numerically diagonalizing the tight-binding model Hamiltonian. For example, Hamiltonians \mathcal{H}_2 , \mathcal{H}_3 , and \mathcal{H}_4 have been shown to host 4, 8, and 16 CZESs in 2D, 3D, and 4D space, respectively [1, 80]. Here, we show that \mathcal{H}_d generally hosts 2^d CZESs ($d \geq 2$) and construct the corresponding analytical wave function.

The construction of CZESs depends on the EZESs analytical solution of h_s along each direction. To construct the CZESs, we expand $\mathcal{H}_d(\mathbf{k}_d)$ at $\mathbf{k}_d = 0$ to the second order of \mathbf{k}_d and replace $\mathbf{k}_d = -i\partial_{\mathbf{r}_d}$, where $\mathbf{r}_d = (r_1, \dots, r_d)$ is the coordinate vector. Under this low-energy expansion, then the EZESs of h_s can be written as (see Eq. (5))

$$|X_{z_s}^{(s)}(r_s)\rangle = f_{z_s}^{(s)}(r_s)|\psi_{z_s}^{(s)}\rangle, \quad (8)$$

where spinor $|\psi_{z_s}^{(s)}\rangle$ is the eigenstate of C_s and satisfies $C_s|\psi_{z_s}^{(s)}\rangle = z_s|\psi_{z_s}^{(s)}\rangle$, with eigenvalue $z_s = \pm 1$, and $f_{z_s}^{(s)}(r_s)$ takes the identical form as $f_z(r)$ in Eq. (5) with an additional dimension label s .

Remarkably, we find that the equation $\mathcal{H}_d(\mathbf{r}_d)\Psi(\mathbf{r}_d) = 0$ has 2^d solutions

$$|\Psi_{z_1, \dots, z_d}(\mathbf{r}_d)\rangle = \prod_{s=1}^d f_{z_s}^{(s)}(r_s)|\psi_{z_1, \dots, z_d}\rangle. \quad (9)$$

Here spinor $|\psi_{z_1, \dots, z_d}\rangle$ belongs to the 2^d common eigenstates of matrices $\{C_1, \dots, C_d\}$, which commute with each other, and $|\psi_{z_1, \dots, z_d}\rangle$ satisfies

$$C_s|\psi_{z_1, \dots, z_d}\rangle = z_s|\psi_{z_1, \dots, z_d}\rangle. \quad (10)$$

To give a concrete example, without loss of generality, we choose

$$\begin{aligned} \gamma_{sa}^{(d)} &= \underbrace{\sigma_3 \otimes \dots \otimes \sigma_3}_{s-1} \otimes \sigma_2 \otimes \underbrace{\sigma_0 \dots \sigma_0}_{d-s}, \\ \gamma_{sb}^{(d)} &= \underbrace{\sigma_3 \otimes \dots \otimes \sigma_3}_{s-1} \otimes \sigma_1 \otimes \underbrace{\sigma_0 \dots \sigma_0}_{d-s}, \\ C_s &= i\gamma_{sa}^{(d)}\gamma_{sb}^{(d)} = \underbrace{\sigma_0 \otimes \dots \otimes \sigma_0}_{s-1} \otimes \sigma_3 \otimes \underbrace{\sigma_0 \dots \sigma_0}_{d-s}, \end{aligned} \quad (11)$$

so that the 2^d common eigenstates of matrices $\{C_1, \dots, C_d\}$ take the form

$$|\psi_{z_1, \dots, z_d}\rangle = \varphi_{z_1} \otimes \dots \otimes \varphi_{z_s} \otimes \dots \otimes \varphi_{z_d}, \quad (12)$$

where $\varphi_{z_s} = (1, 0)^T$ for $z_s = 1$ and $\varphi_{z_s} = (0, 1)^T$ for $z_s = -1$, and the 2^d eigenstates of $|\psi_{z_1, \dots, z_d}\rangle$ form a complete set of basis in 2^d spinor space.

By combining Eqs. (8) and (9), it can be easily verified that

$$h_s(r_s)|\Psi_{z_1, \dots, z_d}(\mathbf{r}_d)\rangle = 0, \quad s = 1, \dots, d, \quad (13)$$

which gives rise to $\mathcal{H}_d(\mathbf{r}_d)|\Psi_{z_1, \dots, z_d}(\mathbf{r}_d)\rangle = 0$. As a wave function that decays along all the directions, $|\Psi_{z_1, \dots, z_d}(\mathbf{r}_d)\rangle$ is localized at the corner, and therefore \mathcal{H}_d hosts 2^d CZESs described by Eq. (9). According to Eq. (9), the localized position of CZES $|\Psi_{z_1, \dots, z_d}(\mathbf{r}_d)\rangle$ in real space is completely determined by its labelled eigenvalues $\{z_1, \dots, z_d\}$. To be specific, when $z_s = -1$ (1), CZES $|\Psi_{z_1, \dots, z_d}(\mathbf{r}_d)\rangle$ is localized close to the corner where $r_s = 0$ (L), with L being the length of the system along r_s . As clearly shown in Eq. (12), the 2^d common eigenstates of $\{C_1, \dots, C_d\}$ are not degenerate with respect to the eigenvalues $\{z_1, \dots, z_d\}$, thus each corner of the hyper cubic space has one CZES.

Since there are $(2d+1)$ anti-commuting Gamma matrices with dimension $2^d \times 2^d$ (see Appendix A), d D Hamiltonian \mathcal{H}_d respects chiral symmetry represented by $\mathcal{C} = \prod_{s=1}^d C_s$, with $\{\mathcal{C}, \mathcal{H}_d\} = 0$. Therefore, the CZESs are also the eigenstate of bulk chiral symmetry \mathcal{C} with the eigenvalue $z = \prod_{s=1}^d z_s$. With this property, a local perturbation h_p preserving the chiral symmetry \mathcal{C} with $\{h_p, \mathcal{C}\} = 0$ can not remove the zero-energy state localized at a given corner because

$$\begin{aligned} \langle \Psi_{z_1, \dots, z_d} | h_p | \Psi_{z_1, \dots, z_d} \rangle \\ = z \langle \Psi_{z_1, \dots, z_d} | \mathcal{C} h_p + h_p \mathcal{C} | \Psi_{z_1, \dots, z_d} \rangle / 2 = 0. \end{aligned} \quad (14)$$

This analysis is consistent with the fact that the CZESs can survive when adding some additional terms preserving the chiral symmetry to \mathcal{H}_2 [90].

In the above discussion, we construct CZESs under the low-energy continuum model. We emphasize that the presented method of constructing CZESs also applies to the lattice model Hamiltonian. In Appendix C, we construct the CZESs solution in the second quantization formalism.

IV. BOUNDARY HAMILTONIANS

Based on the analytical solution of CZESs, we perform a general boundary projection to derive the boundary Hamiltonian of \mathcal{H}_d , which turns out to be the BBH models of lower dimension and reveals the dimensional hierarchy.

A. Boundary projection

We schematically describe the process of extracting boundary Hamiltonians of \mathcal{H}_d in two steps. First, we solve the m D gapped boundary states of \mathcal{H}_d analytically for $m = d-1, \dots, 1$. Second, we project bulk Hamiltonian \mathcal{H}_d onto the subspace expanded by the obtained boundary states, which leads to the boundary Hamiltonians.

To derive the gapped boundary states wave function of \mathcal{H}_d under appropriate boundary conditions, we decompose Hamiltonian \mathcal{H}_d into real space and momentum

space parts

$$\mathcal{H}_d(\mathbf{r}_n, \mathbf{k}_m) = \bar{\mathcal{H}}_n(\mathbf{r}_n) + \bar{\mathcal{H}}_m(\mathbf{k}_m), \quad (15)$$

where $\mathbf{r}_n = (r_{m+1}, \dots, r_d)$ is the n D real space coordinate vector, $\mathbf{k}_m = (k_1, \dots, k_m)$ is the m D momentum vector, and $d = n + m$. With a similar CZESs construction presented in Sec. III B, it can be shown that $\bar{\mathcal{H}}_n(\mathbf{r}_n)$ also hosts 2^d EZESs ($n = 1$) or CZESs ($n \geq 2$), which are the common eigenstates of matrices $\{C_{m+1}, \dots, C_d\}$. Note that matrices C_{m+1}, \dots, C_d always commute with $\bar{\mathcal{H}}_m(\mathbf{k}_m)$, namely $[C_{m+1}, \dots, C_d, \bar{\mathcal{H}}(\mathbf{k}_m)] = 0$. Therefore, the boundary states of $\mathcal{H}_d(\mathbf{r}_n, \mathbf{k}_m)$, represented by $|\Phi_\alpha(\mathbf{r}_n, \mathbf{k}_m)\rangle$, are the common eigenstates of C_{m+1}, \dots, C_d and $\bar{\mathcal{H}}(\mathbf{k}_m)$ with the requirements

$$\begin{aligned} \bar{\mathcal{H}}(\mathbf{r}_n)|\Phi_\alpha(\mathbf{r}_n, \mathbf{k}_m)\rangle &= 0, \\ \bar{\mathcal{H}}(\mathbf{k}_m)|\Phi_\alpha(\mathbf{r}_n, \mathbf{k}_m)\rangle &= E(\mathbf{k}_m)|\Phi_\alpha(\mathbf{r}_n, \mathbf{k}_m)\rangle, \end{aligned} \quad (16)$$

which gives rise to

$$\mathcal{H}_d(\mathbf{r}_n, \mathbf{k}_m)|\Phi_\alpha(\mathbf{r}_n, \mathbf{k}_m)\rangle = E(\mathbf{k}_m)|\Phi_\alpha(\mathbf{r}_n, \mathbf{k}_m)\rangle. \quad (17)$$

Distinguished from the gapless boundary states of topological insulators [91, 92], these boundary states are gapped and extended over the whole boundary Brillouin zone, and therefore can be exactly described by a lattice Hamiltonian.

The boundary Hamiltonian can be extracted by projecting bulk Hamiltonian \mathcal{H}_d onto the subspace expanded by the zero-energy states of $\bar{\mathcal{H}}(\mathbf{r}_n)$. To illustrate this process, we take $d = 2$ and $d = 3$ for examples in the following.

B. BBH models in $d = 2$ and $d = 3$

1. 2D BBH model

When $d = 2$, \mathcal{H}_d in Eq. (6) is specified by

$$\begin{aligned} \mathcal{H}_2(\mathbf{k}_2) &= \sum_{s=1}^2 h_s(k_s), \\ h_s(k_s) &= M_s(k_s)\gamma_{sa}^{(2)} + \lambda_s \sin k_s \gamma_{sb}^{(2)}, \end{aligned} \quad (18)$$

which yields $C_s = i\gamma_{sa}^{(2)}\gamma_{sb}^{(2)}$. When taking open and periodic boundary conditions, respectively, along $s = 2$ and 1 directions, $\mathcal{H}_2(r_2, k_1)$ hosts gapped edge states [1, 83]. Since the EZESs of h_2 are the eigenstates of C_2 and $[C_2, h_1] = 0$, the gapped edge states of $\mathcal{H}_2(r_2, k_1)$ are the common eigenstates of C_2 and h_1 [6, 93, 94]

$$\begin{aligned} |\Phi_{z_2}(r_2, k_1)\rangle &= f_{z_2}^{(2)}(r_2)P_{z_2}^{(2)}|\phi(k_1)\rangle, \\ h_1(k_1)|\phi(k_1)\rangle &= \pm E_1(k_1)|\phi(k_1)\rangle, \end{aligned} \quad (19)$$

where edge projection operator is $P_{z_2}^{(2)} = (1 + z_2 C_2)/2$, and states $|\Phi_{-}(r_2, k_1)\rangle$ and $|\Phi_{+}(r_2, k_1)\rangle$ are localized

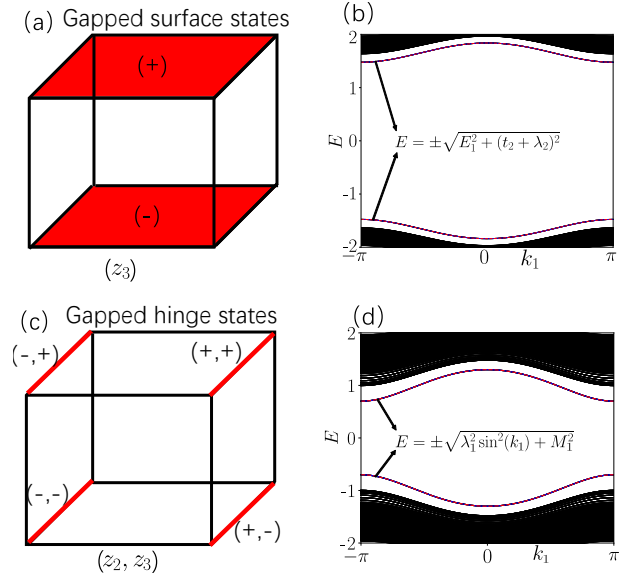


FIG. 2. (a) Schematic illustration of the gapped surface states labeled by the eigenvalue (z_3) of C_3 . (b) The energy spectrum along k_1 for a slab geometry of the system and we take $k_2 = 0$. (c) Schematic illustration of the gapped hinge states labeled by eigenvalues (z_2, z_3) of (C_2, C_3) . (d) The energy spectrum along k_1 for a nanowire geometry of the system. In (c) and (d), the energy spectrum of the in-gap red bands (red lines), corresponding to the gapped boundary states, can be accurately captured by the analytical results (dashed blue lines). For (c) and (d), we take the model parameters as $t_s = 0.3, \lambda_s = 1$ with $s = 1, 2, 3$.

close to edge $r_2 = 0$ and $r_2 = L$, respectively. For a generic case, $|\phi(k_1)\rangle$ is the superposition of eigenstates of C_2 with eigenvalues of 1 and -1 . After the projection, the obtained state $|\Phi_{z_2}(r_2, k_1)\rangle$ is the eigenstate of C_2 with eigenvalue z_2 .

The edge Hamiltonian can be obtained by projecting \mathcal{H}_2 onto the subspace defined by $P_{z_2}^{(2)}$. For example, the edge Hamiltonian for edge $r_2 = 0$ can be written as

$$\begin{aligned} \tilde{h}_1(k_1) &= P_-^{(2)}\mathcal{H}_2P_-^{(2)} \\ &= M_1(k_1)\tilde{\gamma}_{1a}^{(2)} + \lambda_1 \sin k_1 \tilde{\gamma}_{1b}^{(2)}, \end{aligned} \quad (20)$$

where $\tilde{\gamma}_{1a,1b}^{(2)} = P_-^{(2)}\gamma_{1a,1b}^{(2)}P_-^{(2)}$. As $[P_-^{(2)}, h_2] = 0$ and $(P_-^{(2)})^2 = P_-^{(2)}$, we have $\{\tilde{\gamma}_{1a}^{(2)}, \tilde{\gamma}_{1b}^{(2)}\} = 0$ and $(\tilde{\gamma}_{1a,1b}^{(2)})^2 = P_-^{(2)}$. After projecting onto the non-zero block of $P_-^{(2)}$ [6, 95], $\tilde{\gamma}_{1a}^{(2)}$ and $\tilde{\gamma}_{1b}^{(2)}$ form the Clifford algebra and the 2×2 edge Hamiltonian $\tilde{h}_1(k_1)$ behaves as a two-band SSH model. With the same physics, the other edges also behave as the two-band SSH model.

2. 3D BBH model

When $d = 3$, \mathcal{H}_d is given by

$$\mathcal{H}_3(\mathbf{k}_3) = \sum_{s=1}^3 h_s(k_s), \quad (21)$$

$$h_s(k_s) = M_s(k_s)\gamma_{sa}^{(3)} + \lambda_s \sin k_s \gamma_{sb}^{(3)},$$

which gives $C_s = i\gamma_{sa}^{(3)}\gamma_{sb}^{(3)}$. Under the periodic and open boundary conditions, respectively, along $s = 1, 2$ and $s = 3$ directions, we decompose \mathcal{H}_3 as $\mathcal{H}_3(r_3, k_1, k_2) = h_3(r_3) + h_{12}(k_1, k_2)$, with $h_{12} = h_1 + h_2$. Similarly, the gapped surface states of $\mathcal{H}_3(r_3, k_1, k_2)$, schematically illustrated in Fig. 2(a), are the common eigenstates of C_3 and h_{12}

$$\begin{aligned} |\Phi_{z_3}(r_3, k_1, k_2)\rangle &= f_{z_3}^{(3)}(r_3)P_{z_3}^{(3)}|\phi(k_1, k_2)\rangle, \\ h_{12}(k_1, k_2)|\phi(k_1, k_2)\rangle &= E(k_1, k_2)|\phi(k_1, k_2)\rangle, \end{aligned} \quad (22)$$

where surface projection operator is $P_{z_3}^{(3)} = (1 + z_3 C_3)/2$, and the surface energy spectrum is $E = \pm\sqrt{E_1^2 + E_2^2}$, as shown in Fig. 2(b).

Similar to the $d = 2$ case, the surface Hamiltonian for surface $r_3 = 0$ can be written as

$$\begin{aligned} \tilde{h}_{12}(k_1, k_2) &= P_-^{(3)}\mathcal{H}_3P_-^{(3)} \\ &= \sum_{s=1}^2 M_s(k_s)\tilde{\gamma}_{sa}^{(3)} + \lambda_s \sin k_s \tilde{\gamma}_{sb}^s, \end{aligned} \quad (23)$$

where we have defined $\tilde{\gamma}_{sa, sb}^{(3)} = P_-^{(3)}\gamma_{sa, sb}^{(3)}P_-^{(3)}$. Projecting onto the non-zero block of P_-^3 , the 4×4 surface Hamiltonian $\tilde{h}_{12}(k_1, k_2)$ takes completely identical form as the 2D BBH model Hamiltonian \mathcal{H}_2 .

To further extract the hinge Hamiltonian, we take open (periodic) boundary conditions, respectively, along $s = 2, 3$ ($s = 1$) directions, under which we decompose \mathcal{H}_3 as $\mathcal{H}_3(r_2, r_3, k_1) = h_{23}(r_2, r_3) + h_1(k_1)$, with $h_{23} = h_2 + h_3$. The gapped hinge states of $\mathcal{H}_3(r_2, r_3, k_1)$, schematically illustrated in Fig. 2(c), are the common eigenstates of $C_{2,3}$ and h_1

$$\begin{aligned} |\Phi_{z_2, z_3}(r_2, r_3, k_1)\rangle &= \prod_{s=2}^3 f_{z_s}^{(s)}P_{z_s}^{(s)}|\phi(k_1)\rangle, \\ h_1(k_1)|\phi(k_1)\rangle &= \pm E_1(k_1)|\phi(k_1)\rangle, \end{aligned} \quad (24)$$

where $P_{z_s}^{(s)} = (1 + z_s C_s)/2$ and the gapped hinge energy spectrum is $E = \pm E_1$, as shown in Fig. 2(d). When $(z_2, z_3) = \{(-, -), (-, +), (+, -), (+, +)\}$, gapped hinge state $|\Phi_{z_2, z_3}(r_2, r_3, k_1)\rangle$ is localized close to the hinges $(r_2, r_3) = \{(0, 0), (0, L), (L, 0), (L, L)\}$, respectively.

The hinge Hamiltonian for hinge $(r_2, r_3) = (0, 0)$ can be written as

$$\begin{aligned} \tilde{h}_1(k_1) &= P_{--}\mathcal{H}_3P_{--} \\ &= M_1(k_1)\tilde{\gamma}_{1a}^{(3)} + \lambda_1 \sin k_1 \tilde{\gamma}_{1b}^{(3)}, \end{aligned} \quad (25)$$

where hinge projection operator is $P_{z_2 z_3} = \prod_{s=2}^3 P_{z_s}^{(s)}$ and $\tilde{\gamma}_{1a, 1b}^{(3)} = P_{--}\gamma_{1a, 1b}^{(3)}P_{--}$. Distinguished from $P_-^{(3)}$, the non-zero block of P_{--} is 2×2 as P_{--} is the product of two projection operators. Thus when projecting onto the non-zero block of P_{--} , $\tilde{h}_1(k_1)$ takes the exact form of a two-band SSH model.

TABLE I. The hierarchy of the BBH model in arbitrary dimensions. The second row denotes the dimension of the bulk or boundary of the system. The third row lists the bulk Hamiltonian \mathcal{H}_d and boundary Hamiltonians $\tilde{\mathcal{H}}_1, \dots, \tilde{\mathcal{H}}_{d-1}$ with the space dimension in the second row. The fourth row represents the matrix dimension for the Hamiltonians in the third row. The fifth row denotes the number of the CZESs or EZESs for the Hamiltonians in the third row. The sixth row denotes the used boundary projectors to extract the boundary Hamiltonians in the second row. The seventh row denotes the number of configurations of the boundary projections listed in the sixth row.

	bulk	boundary				
dimensions	d	$d-1$	$d-2$	\dots	2	1
Hamiltonians	\mathcal{H}_d	$\tilde{\mathcal{H}}_{d-1}$	$\tilde{\mathcal{H}}_{d-2}$	\dots	$\tilde{\mathcal{H}}_2$	$\tilde{\mathcal{H}}_1$
matrices dimension	2^d	2^{d-1}	2^{d-2}	\dots	2^2	2^1
number of CZESs or EZESs	2^d	2^{d-1}	2^{d-2}	\dots	2^2	2^1
boundary projectors		P_{z_d}	$P_{z_{d-1}z_d}$	\dots	$P_{z_3 \dots z_d}$	$P_{z_2 \dots z_d}$
number of configurations		2^1	2^2	\dots	2^{d-2}	2^{d-1}

C. Generalization to arbitrary dimension

We now show that the mD boundary Hamiltonians of \mathcal{H}_d take completely identical form as the mD BBH model Hamiltonian \mathcal{H}_m in the following.

Following Eq. (15), $\tilde{\mathcal{H}}_n$ hosts 2^d CZESs which are the common eigenstates of $\{C_{m+1}, \dots, C_d\}$ and can be written as

$$|\Psi_{z_{m+1}, \dots, z_d}(\mathbf{r}_n)\rangle = \prod_{q=m+1}^d f_{z_q}^{(q)}(r_q)|\psi_{z_{m+1}, \dots, z_d}\rangle. \quad (26)$$

The zero-energy subspace expanded by the CZESs of $\tilde{\mathcal{H}}_n(\mathbf{r}_n)$ can be defined by the boundary projection operator

$$P_{z_{m+1} \dots z_d} = \prod_{q=m+1}^d (1 + z_q C_q)/2. \quad (27)$$

The gapped boundary states of $\mathcal{H}_d(\mathbf{r}_n, \mathbf{k}_m)$ are the common eigenstates of $C_{m+1, \dots, d}$ and $\tilde{\mathcal{H}}_m$

$$\begin{aligned} |\Phi_{z_{m+1} \dots z_d}(\mathbf{r}_n, \mathbf{k}_m)\rangle &= \prod_{q=m+1}^d f_{z_q}^{(q)}(r_q)P_{z_{m+1} \dots z_d}|\phi(\mathbf{k}_m)\rangle, \\ \tilde{\mathcal{H}}_m(\mathbf{k}_m)|\phi(\mathbf{k}_m)\rangle &= E(\mathbf{k}_m)|\phi(\mathbf{k}_m)\rangle, \end{aligned} \quad (28)$$

where $E(\mathbf{k}_m) = \pm\sqrt{\sum_{s=1}^m E_s^2(k_s)}$. For different eigenvalues configurations of $(z_{m+1}\cdots z_d)$, state $|\Phi_{z_{m+1}\cdots z_d}(\mathbf{r}_n, \mathbf{k}_m)\rangle$ is localized close to different boundaries.

Boundary Hamiltonians can be derived by projecting \mathcal{H}_d onto the zero-energy subspace defined by $P_{z_{m+1}\cdots z_d}$. For example, the boundary Hamiltonian for boundary $r_{m+1,\dots,d} = 0$ can be extracted as

$$\begin{aligned}\tilde{\mathcal{H}}_m(\mathbf{k}_m) &= P_{\dots-}\mathcal{H}_dP_{\dots-} \\ &= \sum_{l=1}^m M_l(k_l)\tilde{\gamma}_{la}^{(d)} + \lambda_l \sin(k_l)\tilde{\gamma}_{lb}^{(d)},\end{aligned}\quad (29)$$

where $\tilde{\gamma}_{la,lb}^{(d)} = P_{\dots-}\gamma_{la,lb}^{(d)}P_{\dots-}$. As $[P_{\dots-}, \gamma_{la,lb}^{(d)}] = 0$, we have $\{\tilde{\gamma}_u^{(d)}, \tilde{\gamma}_{u'}^{(d)}\} = 2\delta_{uu'}P_{\dots-}$ for $u, u' = 1a, \dots, ma, 1b, \dots, mb$. After projecting onto the non-zero block of $P_{\dots-}$, corresponding to the eigenvalues $z_{m+1,\dots,d} = -1$, $\{\tilde{\gamma}_{1a,\dots,ma}^{(d)}, \tilde{\gamma}_{1b,\dots,mb}^{(d)}\}$ form Clifford algebra and boundary Hamiltonian $\tilde{\mathcal{H}}_m$ takes the exact form of the m D BBH model \mathcal{H}_m . We note that the derived boundary Hamiltonian $\tilde{\mathcal{H}}_m$ is related to the higher-order band inversion surfaces given by a special region in the Brillouin zone where $M_s(k_s) = 0$ for $s = 1, \dots, d$ as studied in [39]

The multidimensional boundary states of the BBH model reflect the dimensional hierarchy, summarized in Table I. Meanwhile, there are rich topological transitions for the BBH model \mathcal{H}_d . When $|t_s| = |\lambda_s|$ for $s = 1, \dots, d$, the energy gap of \mathcal{H}_d closes, associated with bulk topological phase transition. When $d - n$ pairs of parameters (t_s, λ_s) satisfy $|t_s| = |\lambda_s|$ and the other n pairs of parameters $(t_{s'}, \lambda_{s'})$ satisfy $|t_{s'}| < |\lambda_{s'}|$, the energy gap of certain $(d - n)$ D boundary closes, corresponding to a boundary topological phase transition. Both the bulk and boundary topological phase transitions can remove the corner states.

V. DISCUSSION AND CONCLUSION

In summary, we generalize the BBH model to arbitrary dimensions and reveal their dimensional hierarchy. For the BBH in arbitrary dimensions, the analytical solution of CZESs can be directly constructed. Based on the analytical solution of CZESs, we develop a general boundary projection method to exact the boundary Hamiltonians, which turns out to be the BBH model of lower dimension and unveils the inherent hierarchy of the BBH model.

For the 2D and 3D BBH models, the nontrivial topology can be characterized by the invariants such as nested Wilson loop, multipole moment calculated based on the many-body wave function [96, 97], and recently proposed chiral multipole number [36]. Although these invariants can be generalized to higher-dimensional systems, it is generally hard to numerically calculate these topological invariants in a system with a dimension larger than

three. Since the d D BBH model is constructed by the combination of the 1D extended SSH model along different directions, the nontrivial topology of the BBH models in arbitrary dimension can be naturally characterized by the topological invariant $\nu = \prod_{i=1}^d \nu_i$, where $\nu_i = 1$ ($\nu_i = 0$) corresponding to the presence (absence) of the end zero-energy states for h_i . We note that a similar topological invariant was defined to characterize a class of higher-order topological phases in arbitrary dimensions with arbitrary orders [39].

In \mathcal{H}_d , although we use the Gamma matrices that anti-commute with each other, this condition can be relaxed to obtain CZESs. In the process of constructing CZESs, we can find that as long as matrices $\{C_1, \dots, C_d\}$ commute with each other, 2^d CZESs can be constructed in the same way for Hamiltonian \mathcal{H}_d , where the 2D case was studied in the work [83]. Therefore, our construction method of CZESs applies to a large class of HOTPs which are stacked by the 1D SSH model along different directions. On the other hand, we only consider the nearest neighboring hopping couplings in \mathcal{H}_d . It was shown that the long-range hopping in the BBH model can give rise to multiple corner zero-energy states at each corner [36]. We emphasize that our theory of constructing corner zero-energy states by the end zero-energy states of different directions is still valid when considering long-range hopping couplings as long as the Bloch Hamiltonian can be separated as $\mathcal{H}_d(\mathbf{k}_d) = \sum_{s=1}^d h_s(k_s)$.

The topological property of Hamiltonian \mathcal{H}_d does not depend on the chosen physical basis. If \mathcal{H}_d is written in the superconducting Bogoliubov-de Gennes basis, the generalized BBH models describe higher-order topological superconductors featuring Majorana corner states, which could be used to perform topological quantum computation [98]. We note that the 2D BBH model in the superconducting system has been studied in the literature [12, 99]

Recent advances in synthetic dimensions provide a feasible way to investigate higher-dimensional topological physics in lower dimensionality by means of additional parameter space. For example, the 4D quantum Hall effect has been realized in photonic crystals [100] and cold atom systems [101] by utilizing synthetic dimensions. In addition, the higher-dimensional system in electric circuits can be flexibly constructed by connecting nonlocal sites, which provides a good platform to study the higher-dimensional physics [102–104]. Thus, the higher-dimensional BBH model could be simulated in these artificial systems.

VI. ACKNOWLEDGMENTS

We thank Xin Liu and Xiao-Hong Pan for their helpful discussions. This work is supported by Key Research and Development Program of Hubei Province (Grant No. 2022BAA017) and start-up funding of Wuhan University.

Appendix A: Clifford algebra and Gamma matrices

For the complex Clifford algebra Cl_{2d} , there are $2d$ generators, labelled as e_j for $j = 1, \dots, 2d$, which satisfy the anti-commutation relation $\{e_j, e_{j'}\} = 2\delta_{jj'}$. Another operator anti-commutes with the $2d$ generators and can be written as

$$e_{2d+1} = i^n e_1 e_2, \dots, e_{2d}, \{e_{2d+1}, e_j\} = 0, e_{2d+1}^2 = 1. \quad (\text{A1})$$

The $(2d+1)$ anti-commuting operators $e_{1, \dots, 2d+1}$ can be represented in terms of anti-commuting $2^d \times 2^d$ Gamma matrices $\gamma_{1, 2, \dots, 2d+1}^{(d)}$, which are the direct product of d sets of Pauli matrices and 2×2 identify matrix and satisfy $(\gamma_j^{(d)})^2 = 1, (\gamma_j^{(d)})^\dagger = \gamma_j^{(d)}$.

When $d=1$, $\gamma_{1,2,3}^{(1)}$ correspond to the three Pauli matrices $\sigma_{1,2,3}$. When $d=2$, $\gamma_{1,2,3,4,5}^{(2)}$ correspond to five anti-commuting Dirac matrices, which can be chosen as

$$\begin{aligned} \gamma_{1,2,3}^{(2)} &= \sigma_3 \otimes \sigma_{1,2,3}, \gamma_4^{(2)} = \sigma_1 \otimes \sigma_0, \\ \gamma_5^{(2)} &= -\gamma_1^{(2)} \gamma_2^{(2)} \gamma_3^{(2)} \gamma_4^{(2)} = \sigma_2 \otimes \sigma_0. \end{aligned} \quad (\text{A2})$$

The anti-commuting $2^d \times 2^d$ Gamma matrices $\gamma_{1, 2, \dots, 2d+1}^{(2d)}$ can be generically obtained according to the iteration relation

$$\begin{aligned} \gamma_{1, 2, \dots, 2d-1}^{(d)} &= \sigma_3 \otimes \gamma_{1, 2, \dots, 2d-1}^{(d-1)}, \\ \gamma_{2d}^{(d)} &= \sigma_1 \otimes I, \gamma_{2d+1}^{(d)} = \sigma_2 \otimes I, \end{aligned} \quad (\text{A3})$$

where I denotes the $2^{d-1} \times 2^{d-1}$ identify matrix.

Appendix B: 1D extended SSH model

We present the calculation of the winding number and EZESs wave function for the 1D extended SSH model. Following the extended SSH model Hamiltonian in Eq. (1), the energy spectrum of h is $\pm E_0 = \pm \sqrt{(t + \lambda \cos k)^2 + (\lambda \sin k)^2}$, then h can be normalized as

$$\begin{aligned} \bar{h} &= h/E_0 \\ &= \cos \varphi \gamma_a^{(d)} + \sin \varphi \gamma_b^{(d)}, \end{aligned} \quad (\text{B1})$$

with $\cos \varphi = (t + \lambda \cos k)/E_0$ and $\sin \varphi = \lambda \sin k/E_0$. The winding number contributed by the occupied states

of $h(k)$ is [105]

$$\begin{aligned} \nu &= \frac{1}{4i\pi} \int_{-\pi}^{\pi} \text{Tr}[C \bar{h} \partial_k \bar{h}] dk \\ &= \frac{1}{4i\pi} \int_{-\pi}^{\pi} \text{Tr}[(\cos \varphi \partial_k \cos \varphi + \sin \varphi \partial_k \sin \varphi) C + \\ &\quad (\cos \varphi \partial_k \sin \varphi - \sin \varphi \partial_k \cos \varphi) C \gamma_1^{(d)} \gamma_2^{(d)}] dk \quad (\text{B2}) \\ &= \frac{2^d}{4\pi} \int_{-\pi}^{\pi} (\cos \varphi \partial_k \sin \varphi - \sin \varphi \partial_k \cos \varphi) dk \\ &= \frac{2^d}{4\pi} \int_{-\pi}^{\pi} \partial_k \varphi dk. \end{aligned}$$

Here, we have used the traceless property of matrix C . When $|t| < |\lambda|$, the integration in Eq. (B2) gives $\nu = 2^{(d-1)}$, otherwise $\nu = 0$.

The winding number $\nu = 2^{(d-1)}$ implies that h hosts $2^{(d-1)}$ EZESs at each end under the open boundary condition. Expanding h at $k = 0$ (supposing that E_0 takes minimum value at $k = 0$) to the second order of k and replacing $k \rightarrow -i\partial_r$, we have

$$h(r) = (m + \lambda/2\partial_r^2) \gamma_a^{(d)} - i\lambda \partial_r \gamma_b^{(d)}, \quad (\text{B3})$$

with $m = t + \lambda$. Considering the semi-infinite system ($r > 0$), the EZESs localized close to $r = 0$ can be derived by solving the equation

$$(m + \lambda/2\partial_r^2) \gamma_a^{(d)} |X_\alpha(r)\rangle - i\lambda \partial_r \gamma_b^{(d)} |X_\alpha(r)\rangle = 0. \quad (\text{B4})$$

Multiplying both sides by $\gamma_1^{(d)}$ in Eq. (B4) yields

$$(m + \lambda/2\partial_r^2) |X_\alpha(r)\rangle = \lambda \partial_r C |X_\alpha(r)\rangle. \quad (\text{B5})$$

Therefore, state $|X_\alpha(r)\rangle$ is the eigenstate of chiral symmetry C and is labeled by the chiral symmetry eigenvalue $z = \pm 1$. We set the trial wave function $|X_z(r)\rangle = e^{\xi_z r} |\psi_z\rangle$, where ξ_z is a complex number, and spinor $|\psi_z\rangle$ satisfies $C|\psi_z\rangle = z|\psi_z\rangle$. Inserting this ansatz solution into Eq. (B5), we have

$$\lambda/2\xi_z^2 - z\lambda\xi + m = 0, \quad (\text{B6})$$

which gives two roots $\xi_z^{1,2} = \frac{z\lambda \pm \sqrt{\lambda^2 - 2m\lambda}}{\lambda}$. When $|t| < |\lambda|$, the real part of $\xi_z^{1,2}$ are negative and positive when $z = -1$ and $z = 1$, respectively. Under the boundary conditions $|X_z(0)\rangle = |X_z(\infty)\rangle = 0$, the wave function of the EZESs can be written as

$$\begin{aligned} |X_-(r)\rangle &= f_-(r) |\psi_-\rangle, \\ f_-(r) &= \mathcal{N}_-(e^{\xi_-^1 r} - e^{\xi_-^2 r}), \end{aligned} \quad (\text{B7})$$

where \mathcal{N}_- is the normalization factor. Similarly, if we consider the semi-system $r < 0$, the EZESs localized close to $r = 0$ is the eigenstate of C with eigenvalue $z = 1$. Therefore, for a finite system with length L , the EZESs localized close to the end $r = 0$ and $r = L$ are the eigenstates of C , with eigenvalue $z = -1$ and $z = 1$,

respectively. Analogously, the wave function of CZESs localized at $r = L$ can be written as

$$\begin{aligned} |X_+(r)\rangle &= f_+(r)|\psi_-\rangle, \\ f_+(r) &= \mathcal{N}_+(e^{\xi_+^\dagger(r-L)} - e^{\xi_+^2(r-L)}), \end{aligned} \quad (\text{B8})$$

where \mathcal{N}_+ is the normalization factor.

Appendix C: The CZESs solution in the second quantization formalism

We show that the constructed wave function in Eq. (9) can also be obtained using the second quantization formalism. We rewrite the Hamiltonian in Eq. (6) as

$$\begin{aligned} \mathcal{H}^{(d)} &= \sum_{\alpha,\beta,\mathbf{k}_d} \mathcal{H}_{\alpha,\beta}^{(d)}(\mathbf{k}_d) c_{\alpha,\mathbf{k}_d}^\dagger c_{\beta,\mathbf{k}_d}, \\ \mathcal{H}_{\alpha,\beta}^{(d)}(\mathbf{k}_d) &= \sum_{s=1}^d h_{\alpha,\beta}^{(s)}(k_s), \\ h^{(s)}(k_s) &= M_s(k_s)\gamma_{sa}^{(d)} + \lambda_s \sin k_s \gamma_{sb}^{(d)}, \end{aligned} \quad (\text{C1})$$

where indexes α and β denote the inner degree of freedom of Hamiltonian with $\alpha, \beta = 1, \dots, 2^d$, $\mathbf{k}_d = (k_1, \dots, k_d)$ is d D momentum vector, index s denotes the different directions, and $c_{\alpha,\mathbf{k}_d}^\dagger$ (c_{β,\mathbf{k}_d}) denotes the creation (annihilation) operator at \mathbf{k}_d with sublattice α (β). $h^{(s)}$ is the 1D extended SSH model and respects chiral symmetry $C_s = i\gamma_{sa}^{(d)}\gamma_{sb}^{(d)}$.

By performing Fourier transformation for \mathcal{H}_d , we obtain the tight-binding model Hamiltonian

$$\begin{aligned} \mathcal{H}^{(d)} &= \sum_{\alpha,\beta,\mathbf{i}_d,\mathbf{i}'_d} \mathcal{H}_{\alpha,\beta}^{(d)}(\mathbf{i}_d,\mathbf{i}'_d) c_{\alpha,\mathbf{i}_d}^\dagger c_{\beta,\mathbf{i}'_d}, \\ \mathcal{H}_{\alpha,\beta}^{(d)}(\mathbf{i}_d,\mathbf{i}'_d) &= \sum_{s=1}^d h_{\alpha,\beta}^{(s)}(i_s,i'_s), \end{aligned} \quad (\text{C2})$$

$$\begin{aligned} h^{(s)}|\Psi\rangle &= \sum_{\alpha,\beta,\eta,\mathbf{i}_d,\mathbf{i}'_d,\mathbf{i}''_d} h_{\alpha,\beta}^{(s)}(i_s,i'_s) c_{\alpha,\mathbf{i}_d}^\dagger c_{\beta,\mathbf{i}'_d} \prod_{s'=1}^d f^{(s')}(i''_{s'}) \chi_\eta c_{\eta,\mathbf{i}''_d}^\dagger |0\rangle \\ &= \sum_{\alpha,\beta,\mathbf{i}_d,\mathbf{i}'_d} h_{\alpha,\beta}^{(s)}(i_s,i'_s) f^{(s)}(i'_s) \chi_\beta \prod_{s' \neq s} f^{(s')}(i'_{s'}) c_{\alpha,\mathbf{i}_d}^\dagger |0\rangle. \end{aligned} \quad (\text{C7})$$

Combining with Eq. (C5), we have $h^{(s)}|\Psi_\eta\rangle = 0$. There-

where $\mathbf{i}_d = (i_1, \dots, i_d)$ and $\mathbf{i}'_d = (i'_1, \dots, i'_d)$ denote the coordinate of lattice site in the d D system, i_s and i'_s take the integer value, and $c_{\alpha,\mathbf{i}_d}^\dagger$ (c_{β,\mathbf{i}'_d}) is the creation (annihilation) operator at site \mathbf{i}_d (\mathbf{i}'_d) with sublattice α (β).

In the second quantization formalism, the 2^d EZESs of $h^{(s)}$ can be generically written as

$$|X^{(s)}\rangle = \sum_{\mathbf{i}_d,\eta} f^{(s)}(i_s) \chi_\eta c_{\eta,\mathbf{i}_d}^\dagger |0\rangle, \quad (\text{C3})$$

where $\mathbf{i}_d = (i_1, \dots, i_d)$ denotes the lattice coordinate, $f^{(s)}(i_s)$ is the site-dependent wave function, spinor χ belongs to the 2^d common eigenstates of $\{C_1, \dots, C_d\}$ with component χ_η , and $|0\rangle$ denotes the vacuum state.

The Hamiltonian $h^{(s)}$ acts on the EZESs $|X^{(s)}\rangle$ as

$$\begin{aligned} h^{(s)}|X^{(s)}\rangle &= \sum_{\alpha,\beta,\eta,\mathbf{i}_d,\mathbf{i}'_d,\mathbf{i}''_d} h_{\alpha,\beta}^{(s)}(i_s,i'_s) c_{\alpha,\mathbf{i}_d}^\dagger c_{\beta,\mathbf{i}'_d} f^{(s)}(i''_s) \chi_\eta c_{\eta,\mathbf{i}''_d}^\dagger |0\rangle \\ &= \sum_{\alpha,\beta,\mathbf{i}_d,\mathbf{i}'_d} h_{\alpha,\beta}^{(s)}(i_s,i'_s) f^{(s)}(i'_s) \chi_\beta c_{\alpha,\mathbf{i}_d}^\dagger |0\rangle, \end{aligned} \quad (\text{C4})$$

which vanishes if

$$\sum_{\beta,\mathbf{i}'_d} h_{\alpha,\beta}^{(s)}(i_s,i'_s) f^{(s)}(i'_s) \chi_\beta = 0. \quad (\text{C5})$$

For the Hamiltonian $\mathcal{H}^{(d)}$, we construct the corner-localized state

$$|\Psi\rangle = \sum_{\mathbf{i}_d,\eta} \prod_{s=1}^d f^{(s)}(i_s) \chi_\eta c_{\eta,\mathbf{i}_d}^\dagger |0\rangle. \quad (\text{C6})$$

Now we demonstrate that $\mathcal{H}^{(d)}|\Psi\rangle = 0$. Each term $h^{(s)}$, for $s = 1, \dots, d$, acts on the corner-localized state $|\Psi\rangle$ as

Therefore, the state $|\Psi\rangle$ is a CZES of \mathcal{H}^d .

- [1] W. A. Benalcazar, B. A. Bernevig, and T. L. Hughes, Quantized electric multipole insulators, *Science* **357**, 61 (2017).
 [2] W. A. Benalcazar, B. A. Bernevig, and T. L. Hughes, Electric multipole moments, topological multipole moment pumping, and chiral hinge states in crystalline in-

- ulators, *Phys. Rev. B* **96**, 245115 (2017).
 [3] F. Liu and K. Wakabayashi, Novel Topological Phase with a Zero Berry Curvature, *Phys. Rev. Lett.* **118**, 076803 (2017).
 [4] Z. Song, Z. Fang, and C. Fang, $(d-2)$ -Dimensional Edge States of Rotation Symmetry Protected Topolog-

- ical States, *Phys. Rev. Lett.* **119**, 246402 (2017).
- [5] J. Langbehn, Y. Peng, L. Trifunovic, F. von Oppen, and P. W. Brouwer, Reflection-Symmetric Second-Order Topological Insulators and Superconductors, *Phys. Rev. Lett.* **119**, 246401 (2017).
 - [6] E. Khalaf, Higher-order topological insulators and superconductors protected by inversion symmetry, *Phys. Rev. B* **97**, 205136 (2018).
 - [7] M. Geier, L. Trifunovic, M. Hoskam, and P. W. Brouwer, Second-order topological insulators and superconductors with an order-two crystalline symmetry, *Phys. Rev. B* **97**, 205135 (2018).
 - [8] M. Ezawa, Higher-Order Topological Insulators and Semimetals on the Breathing Kagome and Pyrochlore Lattices, *Phys. Rev. Lett.* **120**, 026801 (2018).
 - [9] F. Schindler, Z. Wang, M. G. Vergniory, A. M. Cook, A. Murani, S. Sengupta, A. Y. Kasumov, R. Deblock, S. Jeon, I. Drozdov, H. Bouchiat, S. Guéron, A. Yazdani, B. A. Bernevig, and T. Neupert, Higher-order topology in bismuth, *Nature Physics* **14**, 918 (2018).
 - [10] F. Schindler, A. M. Cook, M. G. Vergniory, Z. Wang, S. S. P. Parkin, B. A. Bernevig, and T. Neupert, Higher-order topological insulators, *Science Advances* **4**, 0346 (2018).
 - [11] B.-Y. Xie, H.-F. Wang, H.-X. Wang, X.-Y. Zhu, J.-H. Jiang, M.-H. Lu, and Y.-F. Chen, Second-order photonic topological insulator with corner states, *Phys. Rev. B* **98**, 205147 (2018).
 - [12] Y. Wang, M. Lin, and T. L. Hughes, Weak-pairing higher order topological superconductors, *Phys. Rev. B* **98**, 165144 (2018).
 - [13] X. Zhu, Tunable Majorana corner states in a two-dimensional second-order topological superconductor induced by magnetic fields, *Phys. Rev. B* **97**, 205134 (2018).
 - [14] R. Queiroz and A. Stern, Splitting the Hinge Mode of Higher-Order Topological Insulators, *Phys. Rev. Lett.* **123**, 036802 (2019).
 - [15] Z. Yan, Higher-Order Topological Odd-Parity Superconductors, *Phys. Rev. Lett.* **123**, 177001 (2019).
 - [16] X. Zhang, H.-X. Wang, Z.-K. Lin, Y. Tian, B. Xie, M.-H. Lu, Y.-F. Chen, and J.-H. Jiang, Second-order topology and multidimensional topological transitions in sonic crystals, *Nature Physics* **15**, 582 (2019).
 - [17] X.-W. Luo and C. Zhang, Higher-Order Topological Corner States Induced by Gain and Loss, *Phys. Rev. Lett.* **123**, 073601 (2019).
 - [18] B.-Y. Xie, G.-X. Su, H.-F. Wang, H. Su, X.-P. Shen, P. Zhan, M.-H. Lu, Z.-L. Wang, and Y.-F. Chen, Visualization of Higher-Order Topological Insulating Phases in Two-Dimensional Dielectric Photonic Crystals, *Phys. Rev. Lett.* **122**, 233903 (2019).
 - [19] C. Yue, Y. Xu, Z. Song, H. Weng, Y.-M. Lu, C. Fang, and X. Dai, Symmetry-enforced chiral hinge states and surface quantum anomalous Hall effect in the magnetic axion insulator $\text{Bi}_{2-x}\text{Sm}_x\text{Se}_3$, *Nature Physics* **15**, 577 (2019).
 - [20] R. Okugawa, S. Hayashi, and T. Nakanishi, Second-order topological phases protected by chiral symmetry, *Phys. Rev. B* **100**, 235302 (2019).
 - [21] T. Liu, Y.-R. Zhang, Q. Ai, Z. Gong, K. Kawabata, M. Ueda, and F. Nori, Second-Order Topological Phases in Non-Hermitian Systems, *Phys. Rev. Lett.* **122**, 076801 (2019).
 - [22] Z. Zhang, M. Rosendo López, Y. Cheng, X. Liu, and J. Christensen, Non-Hermitian Sonic Second-Order Topological Insulator, *Phys. Rev. Lett.* **122**, 195501 (2019).
 - [23] L. Trifunovic and P. W. Brouwer, Higher-Order Bulk-Boundary Correspondence for Topological Crystalline Phases, *Phys. Rev. X* **9**, 011012 (2019).
 - [24] Y. Peng, Floquet higher-order topological insulators and superconductors with space-time symmetries, *Phys. Rev. Research* **2**, 013124 (2020).
 - [25] A. Cerjan, M. Jürgensen, W. A. Benalcazar, S. Mukherjee, and M. C. Rechtsman, Observation of a Higher-Order Topological Bound State in the Continuum, *Phys. Rev. Lett.* **125**, 213901 (2020).
 - [26] R. Chen, C.-Z. Chen, J.-H. Gao, B. Zhou, and D.-H. Xu, Higher-Order Topological Insulators in Quasicrystals, *Phys. Rev. Lett.* **124**, 036803 (2020).
 - [27] C.-B. Hua, R. Chen, B. Zhou, and D.-H. Xu, Higher-order topological insulator in a dodecagonal quasicrystal, *Phys. Rev. B* **102**, 241102(R) (2020).
 - [28] H. Hu, B. Huang, E. Zhao, and W. V. Liu, Dynamical Singularities of Floquet Higher-Order Topological Insulators, *Phys. Rev. Lett.* **124**, 057001 (2020).
 - [29] B. Huang and W. V. Liu, Floquet Higher-Order Topological Insulators with Anomalous Dynamical Polarization, *Phys. Rev. Lett.* **124**, 216601 (2020).
 - [30] Y.-B. Choi, Y. Xie, C.-Z. Chen, J. Park, S.-B. Song, J. Yoon, B. J. Kim, T. Taniguchi, K. Watanabe, J. Kim, K. C. Fong, M. N. Ali, K. T. Law, and G.-H. Lee, Evidence of higher-order topology in multilayer WTe_2 from Josephson coupling through anisotropic hinge states, *Nature Materials* **19**, 974 (2020).
 - [31] R.-X. Zhang, Y.-T. Hsu, and S. Das Sarma, Higher-order topological Dirac superconductors, *Phys. Rev. B* **102**, 094503 (2020).
 - [32] L. Aggarwal, P. Zhu, T. L. Hughes, and V. Madhavan, Evidence for higher order topology in Bi and $\text{Bi}_{10.92}\text{Sb}_{0.08}$, *Nature Communications* **12**, 4420 (2021).
 - [33] E. Khalaf, W. A. Benalcazar, T. L. Hughes, and R. Queiroz, Boundary-obstructed topological phases, *Phys. Rev. Research* **3**, 013239 (2021).
 - [34] Y. Wang, Y. Ke, Y.-J. Chang, Y.-H. Lu, J. Gao, C. Lee, and X.-M. Jin, Constructing higher-order topological states in higher dimensions, *Phys. Rev. B* **104**, 224303 (2021).
 - [35] W. Zhang, D. Zou, Q. Pei, W. He, J. Bao, H. Sun, and X. Zhang, Experimental Observation of Higher-Order Topological Anderson Insulators, *Phys. Rev. Lett.* **126**, 146802 (2021).
 - [36] W. A. Benalcazar and A. Cerjan, Chiral-Symmetric Higher-Order Topological Phases of Matter, *Phys. Rev. Lett.* **128**, 127601 (2022).
 - [37] Y. Tan, Z.-H. Huang, and X.-J. Liu, Two-particle Berry phase mechanism for Dirac and Majorana Kramers pairs of corner modes, *Phys. Rev. B* **105**, L041105 (2022).
 - [38] Z. Lei, Y. Deng, and L. Li, Topological classification of higher-order topological phases with nested band inversion surfaces, *Phys. Rev. B* **106**, 245105 (2022).
 - [39] W. Jia, X.-C. Zhou, L. Zhang, L. Zhang, and X.-J. Liu, Unified characterization for higher-order topological phase transitions, *Phys. Rev. Res.* **5**, L022032 (2023).
 - [40] M. Ezawa, Topological Switch between Second-Order Topological Insulators and Topological Crystalline In-

- sulators, *Phys. Rev. Lett.* **121**, 116801 (2018).
- [41] M. J. Park, Y. Kim, G. Y. Cho, and S. B. Lee, Higher-Order Topological Insulator in Twisted Bilayer Graphene, *Phys. Rev. Lett.* **123**, 216803 (2019).
- [42] X.-L. Sheng, C. Chen, H. Liu, Z. Chen, Z.-M. Yu, Y. X. Zhao, and S. A. Yang, Two-Dimensional Second-Order Topological Insulator in Graphdiyne, *Phys. Rev. Lett.* **123**, 256402 (2019).
- [43] C. Chen, Z. Song, J.-Z. Zhao, Z. Chen, Z.-M. Yu, X.-L. Sheng, and S. A. Yang, Universal Approach to Magnetic Second-Order Topological Insulator, *Phys. Rev. Lett.* **125**, 056402 (2020).
- [44] R.-X. Zhang, F. Wu, and S. Das Sarma, Möbius Insulator and Higher-Order Topology in $\text{MnBi}_{12n}\text{Te}_{3n+1}$, *Phys. Rev. Lett.* **124**, 136407 (2020).
- [45] Y. Ren, Z. Qiao, and Q. Niu, Engineering Corner States from Two-Dimensional Topological Insulators, *Phys. Rev. Lett.* **124**, 166804 (2020).
- [46] B. Liu, L. Xian, H. Mu, G. Zhao, Z. Liu, A. Rubio, and Z. F. Wang, Higher-Order Band Topology in Twisted Moiré Superlattice, *Phys. Rev. Lett.* **126**, 066401 (2021).
- [47] Z. Yan, F. Song, and Z. Wang, Majorana Corner Modes in a High-Temperature Platform, *Phys. Rev. Lett.* **121**, 096803 (2018).
- [48] Q. Wang, C.-C. Liu, Y.-M. Lu, and F. Zhang, High-Temperature Majorana Corner States, *Phys. Rev. Lett.* **121**, 186801 (2018).
- [49] P. Zhang, K. Yaji, T. Hashimoto, Y. Ota, T. Kondo, K. Okazaki, Z. Wang, J. Wen, G. D. Gu, H. Ding, and S. Shin, Observation of topological superconductivity on the surface of an iron-based superconductor, *Science* **360**, 182 (2018).
- [50] X. Zhu, Second-Order Topological Superconductors with Mixed Pairing, *Phys. Rev. Lett.* **122**, 236401 (2019).
- [51] R.-X. Zhang, W. S. Cole, and S. Das Sarma, Helical Hinge Majorana Modes in Iron-Based Superconductors, *Phys. Rev. Lett.* **122**, 187001 (2019).
- [52] Y. Volpez, D. Loss, and J. Klinovaja, Second-Order Topological Superconductivity in π -Junction Rashba Layers, *Phys. Rev. Lett.* **122**, 126402 (2019).
- [53] X.-H. Pan, K.-J. Yang, L. Chen, G. Xu, C.-X. Liu, and X. Liu, Lattice-Symmetry-Assisted Second-Order Topological Superconductors and Majorana Patterns, *Phys. Rev. Lett.* **123**, 156801 (2019).
- [54] X. Wu, W. A. Benalcazar, Y. Li, R. Thomale, C.-X. Liu, and J. Hu, Boundary-Obstructed Topological High- T_c Superconductivity in Iron Pnictides, *Phys. Rev. X* **10**, 041014 (2020).
- [55] Y.-J. Wu, J. Hou, Y.-M. Li, X.-W. Luo, X. Shi, and C. Zhang, In-Plane Zeeman-Field-Induced Majorana Corner and Hinge Modes in an s -Wave Superconductor Heterostructure, *Phys. Rev. Lett.* **124**, 227001 (2020).
- [56] R.-X. Zhang and S. Das Sarma, Intrinsic Time-Reversal-Invariant Topological Superconductivity in Thin Films of Iron-Based Superconductors, *Phys. Rev. Lett.* **126**, 137001 (2021).
- [57] L. Chen, B. Liu, G. Xu, and X. Liu, Lattice distortion induced first- and second-order topological phase transition in a rectangular high- T_c superconducting monolayer, *Phys. Rev. Research* **3**, 023166 (2021).
- [58] X.-J. Luo, X.-H. Pan, and X. Liu, Higher-order topological superconductors based on weak topological insulators, *Phys. Rev. B* **104**, 104510 (2021).
- [59] H. D. Scammell, J. Ingham, M. Geier, and T. Li, Intrinsic first- and higher-order topological superconductivity in a doped topological insulator, *Phys. Rev. B* **105**, 195149 (2022).
- [60] T. Li, M. Geier, J. Ingham, and H. D. Scammell, Higher-order topological superconductivity from repulsive interactions in kagome and honeycomb systems, *2D Materials* **9**, 015031 (2021).
- [61] M. Lin and T. L. Hughes, Topological quadrupolar semimetals, *Phys. Rev. B* **98**, 241103(R) (2018).
- [62] H.-X. Wang, Z.-K. Lin, B. Jiang, G.-Y. Guo, and J.-H. Jiang, Higher-Order Weyl Semimetals, *Phys. Rev. Lett.* **125**, 146401 (2020).
- [63] Z. Wang, D. Liu, H. T. Teo, Q. Wang, H. Xue, and B. Zhang, Higher-order Dirac semimetal in a photonic crystal, *Phys. Rev. B* **105**, L060101 (2022).
- [64] W. A. Benalcazar, T. Li, and T. L. Hughes, Quantization of fractional corner charge in C_n -symmetric higher-order topological crystalline insulators, *Phys. Rev. B* **99**, 245151 (2019).
- [65] H. Watanabe and H. C. Po, Fractional Corner Charge of Sodium Chloride, *Phys. Rev. X* **11**, 041064 (2021).
- [66] M. Jung, Y. Yu, and G. Shvets, Exact higher-order bulk-boundary correspondence of corner-localized states, *Phys. Rev. B* **104**, 195437 (2021).
- [67] S.-B. Zhang, W. B. Rui, A. Calzona, S.-J. Choi, A. P. Schnyder, and B. Trauzettel, Topological and holonomic quantum computation based on second-order topological superconductors, *Phys. Rev. Research* **2**, 043025 (2020).
- [68] S.-B. Zhang, A. Calzona, and B. Trauzettel, All-electrically tunable networks of majorana bound states, *Phys. Rev. B* **102**, 100503(R) (2020).
- [69] T. E. Pahomi, M. Sigrist, and A. A. Soluyanov, Braiding Majorana corner modes in a second-order topological superconductor, *Phys. Rev. Research* **2**, 032068(R) (2020).
- [70] X.-H. Pan, X.-J. Luo, J.-H. Gao, and X. Liu, Detecting and braiding higher-order majorana corner states through their spin degree of freedom, *Phys. Rev. B* **105**, 195106 (2022).
- [71] K. Chen, M. Weiner, M. Li, X. Ni, A. Alù, and A. B. Khanikaev, Fourth-Order Topological Insulator via Dimensional Reduction, *arXiv:1912.06339* (2019).
- [72] M. Serra-Garcia, V. Peri, R. Süsstrunk, O. R. Bilal, T. Larsen, L. G. Villanueva, and S. D. Huber, Observation of a phononic quadrupole topological insulator, *Nature* **555**, 342 (2018).
- [73] S. Mittal, V. V. Orre, G. Zhu, M. A. Gorlach, A. Poddubny, and M. Hafezi, Photonic quadrupole topological phases, *Nature Photonics* **13**, 692 (2019).
- [74] J. Schulz, J. Noh, W. A. Benalcazar, G. Bahl, and G. von Freymann, Photonic quadrupole topological insulator using orbital-induced synthetic flux, *Nature Communications* **13**, 6597 (2022).
- [75] Y. Qi, C. Qiu, M. Xiao, H. He, M. Ke, and Z. Liu, Acoustic Realization of Quadrupole Topological Insulators, *Phys. Rev. Lett.* **124**, 206601 (2020).
- [76] H. Xue, Y. Ge, H.-X. Sun, Q. Wang, D. Jia, Y.-J. Guan, S.-Q. Yuan, Y. Chong, and B. Zhang, Observation of an acoustic octupole topological insulator, *Nature Communications* **11**, 2442 (2020).
- [77] S. Imhof, C. Berger, F. Bayer, J. Brehm, L. W.

- Molenkamp, T. Kiessling, F. Schindler, C. H. Lee, M. Greiter, T. Neupert, and R. Thomale, Topoelectrical-circuit realization of topological corner modes, *Nature Physics* **14**, 925 (2018).
- [78] M. Serra-Garcia, R. Süsstrunk, and S. D. Huber, Observation of quadrupole transitions and edge mode topology in an lc circuit network, *Phys. Rev. B* **99**, 020304(R) (2019).
- [79] J. Bao, D. Zou, W. Zhang, W. He, H. Sun, and X. Zhang, Topoelectrical circuit octupole insulator with topologically protected corner states, *Phys. Rev. B* **100**, 201406(R) (2019).
- [80] W. Zhang, D. Zou, J. Bao, W. He, Q. Pei, H. Sun, and X. Zhang, Topoelectrical-circuit realization of a four-dimensional hexadecapole insulator, *Phys. Rev. B* **102**, 100102(R) (2020).
- [81] W. P. Su, J. R. Schrieffer, and A. J. Heeger, Solitons in Polyacetylene, *Phys. Rev. Lett.* **42**, 1698 (1979).
- [82] C.-A. Li, B. Fu, Z.-A. Hu, J. Li, and S.-Q. Shen, Topological Phase Transitions in Disordered Electric Quadrupole Insulators, *Phys. Rev. Lett.* **125**, 166801 (2020).
- [83] X.-J. Luo, X.-H. Pan, C.-X. Liu, and X. Liu, Higher-order topological phases emerging from su-schrieffer-heeger stacking, *Phys. Rev. B* **107**, 045118 (2023).
- [84] A. P. Schnyder, S. Ryu, A. Furusaki, and A. W. W. Ludwig, Classification of topological insulators and superconductors in three spatial dimensions, *Phys. Rev. B* **78**, 195125 (2008).
- [85] S. Ryu, A. P. Schnyder, A. Furusaki, and A. W. W. Ludwig, Topological insulators and superconductors: tenfold way and dimensional hierarchy, *New Journal of Physics* **12**, 065010 (2010).
- [86] C.-K. Chiu, J. C. Y. Teo, A. P. Schnyder, and S. Ryu, Classification of topological quantum matter with symmetries, *Rev. Mod. Phys.* **88**, 035005 (2016).
- [87] J. C. Y. Teo and C. L. Kane, Topological defects and gapless modes in insulators and superconductors, *Phys. Rev. B* **82**, 115120 (2010).
- [88] R. W. Bomantara, L. Zhou, J. Pan, and J. Gong, Coupled-wire construction of static and floquet second-order topological insulators, *Phys. Rev. B* **99**, 045441 (2019).
- [89] R.-X. Zhang, J. D. Sau, and S. Das Sarma, Kitaev Building-block Construction for Higher-order Topological Superconductors, [arXiv:2003.02559](https://arxiv.org/abs/2003.02559) (2020).
- [90] C.-A. Li and S.-S. Wu, Topological states in generalized electric quadrupole insulators, *Phys. Rev. B* **101**, 195309 (2020).
- [91] M. Z. Hasan and C. L. Kane, Colloquium: Topological insulators, *Reviews of Modern Physics* **82**, 3045 (2010).
- [92] X.-L. Qi and S.-C. Zhang, Topological insulators and superconductors, *Reviews of Modern Physics* **83**, 1057 (2011).
- [93] E. Khalaf, H. C. Po, A. Vishwanath, and H. Watanabe, Symmetry Indicators and Anomalous Surface States of Topological Crystalline Insulators, *Phys. Rev. X* **8**, 031070 (2018).
- [94] E. Roberts, J. Behrends, and B. Béri, Second-order bulk-boundary correspondence in rotationally symmetric topological superconductors from stacked dirac hamiltonians, *Phys. Rev. B* **101**, 155133 (2020).
- [95] C.-K. Chiu, H. Yao, and S. Ryu, Classification of topological insulators and superconductors in the presence of reflection symmetry, *Phys. Rev. B* **88**, 075142 (2013).
- [96] W. A. Wheeler, L. K. Wagner, and T. L. Hughes, Many-body electric multipole operators in extended systems, *Phys. Rev. B* **100**, 245135 (2019).
- [97] B. Kang, K. Shiozaki, and G. Y. Cho, Many-body order parameters for multipoles in solids, *Phys. Rev. B* **100**, 245134 (2019).
- [98] C. Nayak, S. H. Simon, A. Stern, M. Freedman, and S. Das Sarma, Non-Abelian anyons and topological quantum computation, *Rev. Mod. Phys.* **80**, 1083 (2008).
- [99] A. Tiwari, A. Jahin, and Y. Wang, Chiral Dirac superconductors: Second-order and boundary-obstructed topology, *Phys. Rev. Research* **2**, 043300 (2020).
- [100] O. Zilberberg, S. Huang, J. Guglielmon, M. Wang, K. P. Chen, Y. E. Kraus, and M. C. Rechtsman, Photonic topological boundary pumping as a probe of 4D quantum Hall physics, *Nature* **553**, 59 (2018).
- [101] M. Lohse, C. Schweizer, H. M. Price, O. Zilberberg, and I. Bloch, Exploring 4D quantum Hall physics with a 2D topological charge pump, *Nature* **553**, 55 (2018).
- [102] M. Ezawa, Electric circuit simulations of n th-chern-number insulators in $2n$ -dimensional space and their non-hermitian generalizations for arbitrary n , *Phys. Rev. B* **100**, 075423 (2019).
- [103] L. Li, C. H. Lee, and J. Gong, Emergence and full 3D-imaging of nodal boundary Seifert surfaces in 4D topological matter, *Communications Physics* **2**, 135 (2019).
- [104] R. Yu, Y. X. Zhao, and A. P. Schnyder, 4D spinless topological insulator in a periodic electric circuit, *National Science Review* **7**, 1288 (2020).
- [105] L. Zhang, L. Zhang, S. Niu, and X.-J. Liu, Dynamical classification of topological quantum phases, *Science Bulletin* **63**, 1385 (2018).